AoI-Aware Waveform Design for Cooperative Joint Radar-Communications Systems with Online Prediction of Radar Target Property

Zhuofei Li, *Student Member, IEEE,* Fengye Hu, *Senior Member, IEEE,* Qihao Li, *Member, IEEE,* Zhuang Ling, *Member, IEEE,* Zheng Chang, *Senior Member, IEEE,* and Timo Hämäläinen, *Senior Member, IEEE*

***Abstract*—In this paper, we propose a novel age-of-information (AoI)-aware waveform design scheme for the cooperative joint radar-communications (JRC) system, called AoI-aware Online Prediction (A-OnP) scheme. To be specific, we optimize the power allocation of the orthogonal frequency division multiplexing (OFDM) signal. We aim to maximize the radar mutual information (RMI) with considering the communication data rate (CDR) and AoI performance. Specifically, we design a cognitive operating framework for the JRC system, with a particular emphasis on the closed-loop signal processing for online prediction of the radar target scattering coefficient (TSC). Then, considering the obtained TSC prediction result and corresponding communication performance requirement, we optimize the power allocation of the transmit waveform and the signal-to-interference-plus-noise ratio (SINR) threshold of the communication users. Accordingly, we propose a constraints-splitting coordinate descent (CS-CD) method to solve the formulated non-convex problem by strategically splitting the sum-constraints and assign a quota to each channel, where the allocation criteria is automatically decided during iteration. Simulation results demonstrate that, the cooperative radar-centric communication-constrained (RC-CC) waveform outperforms the separately optimized radar-optimal plus communication-optimal (RO-CO) waveform. Additionally, the A-OnP scheme can increase RMI while meeting the communication CDR and AoI requirements.**

***Index Terms*—Age of information (AoI), joint radar-communications (JRC), radar mutual information (RMI), cognitive waveform design.**

I. Introduction

Manuscript received 19 July 2023; revised 30 December 2023, accepted 10 April 2024. This work was supported in part by the scholarship from the China Scholarship Council (No. 202206170004), in part by the Joint Fund for Regional Innovation and Development of the National Natural Science Foundation of China (No.U21A20445), in part by the National Natural Science Foundation of China (No. 62201224, No. 62201148, No. 62071105), in part by the Jilin Province Development and Reform Commission Project (No. 2023C039-1), in part by Jilin Provincial Key Laboratory of Intelligent Sensing and Network Technology (No. 20240302096GX, No. 20230508035RC and No. YDZJ202102CXJD018), in part by the Guangdong Province Basic and Applied Basic Research Foundation (No. 2022KQNCX). (*Corresponding author: Fengye Hu.)*

Zhuofei Li, Fengye Hu, Qihao Li, and Zhuang Ling are with the College of Communication Engineering, Jilin University, Changchun 130012, China (e-mail: lizf21@mails.jlu.edu.cn; hufy@jlu.edu.cn; qihaol@jlu.edu.cn; lingzhuang@jlu.edu.cn).

Zheng Chang is with the School of Computer Science and Engineering, University of Electronic Science and Technology of China, Chengdu 611731, China, and also with the Faculty of Information Technology, University of Jyväskylä, 40014 Jyväskylä, Finland (e-mail: zheng.chang@jyu.fi).

Timo Hämäläinen is with the Faculty of Information Technology, University of Jyväskylä, 40014 Jyväskylä, Finland (e-mail: timo.t.hamalainen@jyu.fi).

JOINT radar and communications (JRC) system gained considerable attention due to its capability to simultaneously perform radar sensing and wireless communication while utilizing shared spectrum and hardware resources [1]–[4]. Orthogonal frequency division multiplexing (OFDM) signal has been proved as a suitable waveform for both radar and communication purposes [5]–[7], which enables efficient utilization of the frequency spectrum with multiple orthogonal subcarriers divisions and scalable interference rejection suitable for various channel conditions and bandwidth requirements [8]. In the context of an increasingly congested electromagnetic spectrum, where many frequency bands are no longer exclusively allocated to radar systems, it is crucial to adopt new waveform optimization methods that ensure satisfactory performance for both radar and communication [9]–[12].

Radar and communication have different objectives in the JRC systems: the primary objective of communication is to ensure accurate and timely information exchange, with a focus on maintaining a high Quality of Service (QoS); while the radar's primary task is to detect, recognize, or track targets within its operational range. When the two systems are cohabitate, the design of the radar waveform may be constrained to avoid interfering with legacy communication systems. Therefore, the waveform design in a joint radar and communication system aims to identify an optimal transmit waveform that maximizes sensing performance while minimizing interference on the communication QoS. Such waveform can be obtained through orthogonal resource allocation approach such as time-division [13], spectral division [14], code division [15], and spatial division [16] or through unified waveform design. The orthogonal resource allocation approach provides simplicity and ease of implementation, allowing radar and communication functions to be deployed and integrated into existing systems without requiring sophisticated waveform redesign. But this approach can not achieve high efficiency of valuable resources and is not efficient for real-time systems where radar and communications should meet a variety of dynamic and unpredictable demands. The unified waveform design approach shares time and frequency resources, where a performance trade-off should be optimized due to their different design objectives [17].

Numerous studies have been conducted to address the difficulties associated with OFDM-based waveform design in the JRC or Dual-functional radar communications (DFRC)

systems. In the seminal work [18], the utilization of radar mutual information (RMI) in the formulation of radar waveforms was first introduced. This pioneering effort demonstrated the efficacy of MI in quantifying the estimation proficiency of radar systems. Empirical evidence in [19] substantiates that the optimization of MI and the concomitant minimization of mean square error (MSE) yield congruent outcomes in waveform design under specified conditions. Significantly, MI exhibits a more concise structure in comparison to alternative metrics, thus facilitating a streamlined analysis of the impact of uncertainty information on radar sensing performance and algorithmic design. C. Shi *et al.* focused on the constraints of a predefined RMI and a desired communications data rate (CDR) to optimize the joint power and subcarriers allocation [14]. F. Wang *et al.* maximized the communication throughput under a minimum signal-to-interference-plus-noise ratio (SINR) constraint for the radar along with power constraints, and found that the sharing-based joint design offers additional gain in spectrum efficiency than allocation-based paradigm [20]. Huang et al. proposed a joint radar-communication model consists of a monostatic radar and a set of communication systems operating in the shared frequency band, and derived the optimal radar waveform for target recognition and detection under communication capacity constraint for each single subcarrier [21]. Huang's work has been extended by [22], where B. Kang *et al.* optimized the waveform power allocation by maximizing the radar SINR subjected to the sum capacity of the communication system. Additionally, T. Tian *et al.* investigated the word error probability (WEP) constraint and the radar signal-to-noise ratio (SNR) to optimize the waveform [23].

However, current works mostly consider merely the traditional communication performance metrics in the JRC system, including the channel capacity or error rate. Meanwhile, there are many real-time applications under joint radar and communication systems, in which the freshness of data packets can be essential. Possible applications include autonomous driving, medical monitoring, extended reality (XR), and so on. Age of information (AoI) is a proper metric reflecting data freshness at the communication destination, which is defined to portray how old the freshest received update is since the moment that this update was generated at the source node [24]. Experiments conducted by [25] verify that traditional communication performance metrics (such as throughput and delay) cannot effectively characterize the information freshness of the system. [26] demonstrate that information freshness reflected by AoI is essential in the autonomous driving scenario where sensing and communication are both reqiured. Optimizing JRC waveform according to the AoI metric can achieve better timeliness for those real-time applications. The AoI metric would urge JRC waveform to take care of poor condition channels in order to guarantee connectivity and data freshness. Thus it is meaningful to investigate a new waveform design method with the communication AoI performance taken into account.

Secondly, it is challenging to effectively reschedule the wireless resources in a dynamic environment. First, targets in radar scenes can have diverse and complex scattering behaviors that are difficult to predict accurately before actual measurements are obtained [27]. Radar scenes consist of various types of targets with different shapes, sizes, and materials. Modeling the scattering behavior of each target accurately in advance is challenging due to the lack of comprehensive prior knowledge about the specific targets present in the scene [28]. Therefore, relying solely on offline prediction value may lead to limited performance in sensing radar targets. It is necessary to learn the features of target scattering coefficients (TSCs) from the radar scene in an online way such that the radar service can capture the actual scattering behavior of targets in real-time, accounting for the specific targets present in the scene and their evolving characteristics. Chen *et al.* [29] exploit the channel temporal correlation to predict radar and communication channels according to the channel aging model, aiming to optimize the radar tracking Cramér-Rao lower bounds (CRLB) performance and communication achievable rate performance with respect to the bandwidth, power, and channel aging time. However, the authors only take advantage of the first transmission block whose estimation result is treated as prior information for all the rest $N-1$ blocks.

Moreover, considering the aforementioned limitations, the inclusion of the additional communication constraint introduces further complexity to the optimization problem, making it challenging to solve. In [22], the optimal point of the problem is found by geometric analysis. There were only one non-convex constraint in [22] so that the authors were able to derive a closed form solution to find the locally optimal point at each iteration. In contrast, this paper adopts a similar system model as [21] and [22], but considers a more realistic scenario and setting separate sum-capacity constraints for each communication user, which leads to a hard non-convex problem that can not be solved by the method proposed in [22].

In summery, all the aforementioned works provide valuable results but pay little attention to the communication data freshness metric and the online prediction of the radar target properties. In this paper, we are dedicated to propose a novel joint waveform design scheme in the JRC system with an emphasis on online prediction of the radar target property, which is called AoI-aware online prediction (A-OnP) waveform design scheme. Specifically, the proposed A-OnP scheme consists of two main modules: the TSC prediction module and the AoI-aware radar power scheduling module. In the TSC prediction module, we utilize each of the historical pulse and gain extra accuracy on TSC prediction through long-term observation. Based on the above prediction, in the AoI-aware radar power scheduling module, we propose an OFDM-based waveform design approach which takes AoI as one of the communication metrics to guarantee the data freshness of each communication user while maximizing the mutual information between radar echo and the sensing target. The following are the paper's primary contributions.

- We derive the precise mathematical expression of the AoI in the JRC system based on OFDM signal, quantitatively analyze the radar interference on the AoI of the communication system, which eventually contributes to

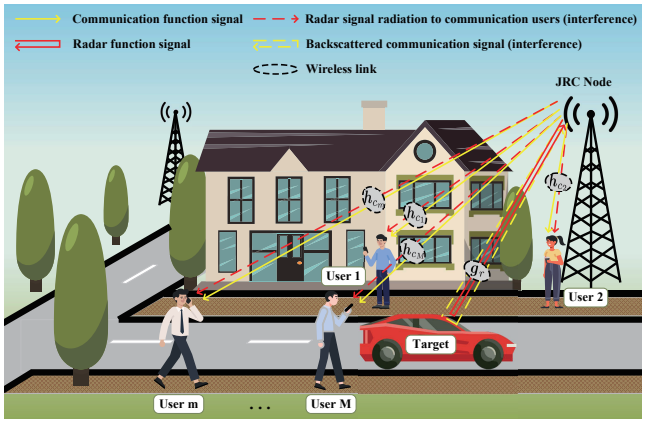

Fig. 1. Joint radar and communications system model.

optimizing the power allocation of the transmit waveform. In particular, we investigate the performance of AoI by evaluating its expectation based on the outage probability of the communication channel in the presence of radar interference.

- We propose a cooperative framework for the JRC system, incorporating closed-loop signal processing for both functions. In this framework, we leverage the temporal correlation of radar target scattering behavior to enable online prediction of the radar TSC. Additionally, we adaptively adjust the communication receiver SINR threshold with regard to the feedback from communication users.
- Considering the formulated nonlinear programming problem, we propose an effective method, called constraint-splitting coordinate descent (CS-CD), to determine the optimal threshold decision and waveform power allocation result. The innovative aspect of this method is manifested in the adaptive decomposition of the non-convex sum constraints, which transfer each sub-problem generated by the traditional coordinate descent (CD) method into a convex problem, thereby effectively solving the original non-convex problem.

In this paper, we explore the single-antenna scenario, where the base station broadcasts signals to the surrounding environment. We optimize the OFDM subcarrier power allocation for a combined signal of radar and communication functionalities. The research presented in this paper is highly applicable to be extended to multi-antenna scenarios, especially in cases where communication and sensing target do not coincide. In such a system model, subcarrier power allocation and beamforming pattern should be jointly optimized to reduce interference in both the spatial and frequency domains, thereby further enhancing the performance of both radar and communication systems.

The rest of this paper is organized as follows. In Section II, we introduce the signal model of the JRC system, and derive the related performance metrics within this model. Section III introduces the operational principles of our proposed cooperative JRC framework and outlines the formulation of the optimization problem within this workflow. Section IV describes the proposed CS-CD method. Section V shows numerical results to verify the proposed method and algorithms. Simulation results are shown in Section V. Finally, Section VI concludes the paper.

II. System Model

As shown in Fig. 1, we consider a JRC system in some city area adjacent to the road, where the JRC nodes (which work as a communication base station equipped with a monostatic radar) are densely deployed, they have dual functions of vehicle sensing and multi-user communication. Each node are responsible for serving a relatively small area where only exists one extended target for sensing and M user equipments (UEs) for communicating. The UEs and the target are scattering in the area and the joint node broadcasts a combined waveform of radar and communication signal. This model is oriented to applications such as Internet of Vehicles (IoV), smart transportation, and smart cities. The BS senses roadside vehicles while ensuring user communication.

Both the radar and communication signals are OFDM signals with N sub-carriers and they operate in a shared frequency band. M communication users split all the channels without overlap, while the radar works in a wide frequency band, covering the whole band range. The communication channel $\boldsymbol{h_{c,m}}$ is considered as Rayleigh fading channels obeying the complex Gaussian distribution. The radar target channel $\boldsymbol{g_r}$ can be described by a wide sense stationary-uncorrelated scattering (WSSUS) model because we consider an extended sensing target in the system [30]. The frequency domain characterization of the extended target can be derived by the Wiener-Khintchine theorem [31].

The joint node transmits a combined signal that operates radar and communication functions simultaneously, causing interference to each other. The radar target backscatters the combined signal, reducing the proportion of useful message in the echo. Communication users can also receive the radar signal, which carries no information and results in a decrease in SINR.

Without loss of generality, the modulation in the baseband is chosen as quadrature phase-shift keying (QPSK). Considering continuous Q pulses with the pulse length of T, then the joint transmit signal of the q-th pulse $d_q(t)$, $\forall t \in [0, T)$ omitting the cyclic prefix (CP) can be expressed by:

$$d_q(t) = \frac{1}{\sqrt{N}} \mathrm{Re}\left\{ \sum_{k=1}^{N} R_k \mathrm{e}^{j2\pi[f_c+(k-1)\Delta f]t} + \sum_{m=1}^{M} \sum_{k\in\mathbb{K}_m} O_{m,k} \mathrm{e}^{j2\pi[f_c+(k-1)\Delta f]t} \right\}, \tag{1}$$

where R_k is the complex amplitude of the radar signal under the k-th sub-carrier, which holds the equation $\sum_{k=1}^{N} |R_k|^2 = \mathrm{P_r}$, $O_{m,k}$ is the complex amplitude of the communication signal of the m-th user under the k-th sub-carrier, which holds the equation $\sum_{m=1}^{M} \sum_{k\in\mathrm{K}_m} |O_{m,k}|^2 = \mathrm{P_c}$, where $\mathrm{P_r}$ and $\mathrm{P_c}$ represents the total transmission power for radar and communication purposes, respectively. $\mathbb{K}_m$ denotes the set of sub-carrier numbers occupied by the m-th user, which holds the equation $\bigcup_m \mathbb{K}_m = \{1, 2, 3, ...N\}$ and $\bigcap_m \mathbb{K}_m = \emptyset$, and

the phase of $O_{m,k}$, $\arg(O_{m,k})$, follows a discrete uniform distribution in $\{\pm\frac{\pi}{2}, \pm\frac{3\pi}{2}\}$ due to QPSK modulation, f_c is the carrier frequency. For simplicity, we refer to each sub-carrier as a channel and each pulse repetition interval (PRI) as a time block in the rest of this paper.

We consider the baseband version of the signal and sample it with sampling rate $f_s = N/T$. The discrete Fourier transform (DFT) of the sampled signal can be written as:

$$\boldsymbol{d}_{s,q} = \boldsymbol{F}\boldsymbol{r}_q + \sum_{m=1}^{M} \boldsymbol{F}\boldsymbol{o}_{m,q} \triangleq \boldsymbol{z}_q + \sum_{m=1}^{M} \boldsymbol{s}_{m,q} \tag{2}$$

where $\boldsymbol{r}_q$ is the sampled transmission signal for radar purpose, and $\boldsymbol{o}_{m,q}$ for communication purpose likewise, $\boldsymbol{F}$ is the unitary DFT matrix.

Thus the signal received by the radar sub-system in the q-th slot can be written as:

$$\boldsymbol{y}_{r,q} = \left(\boldsymbol{Z}_q + \sum_{m=1}^{M} \boldsymbol{S}_{m,q}\right)\boldsymbol{g}_{r,q} + \boldsymbol{n}_{r,q}, \tag{3}$$

where $\boldsymbol{Z}_q = diag(\boldsymbol{z}_q)$, $\boldsymbol{S}_{m,q} = diag(\boldsymbol{s}_{m,q})$, and $\boldsymbol{g}_{r,q} \sim \mathcal{CN}(0, \boldsymbol{G}_r)$ is the TSC of the target, $\boldsymbol{n}_{r,q} \sim \mathcal{CN}(0, \boldsymbol{\Sigma}_{n_r})$ is the system noise of the radar receiver. $\boldsymbol{G}_r, \boldsymbol{\Sigma}_{n_r} \in \mathbb{R}^{N\times N}$ are the covariance matrices of the corresponding parametric distributions. $\boldsymbol{\Sigma}_{n_r} = \boldsymbol{I}_N \cdot \sigma_{n_r}^2$ because the noise samples are independent and identically distributed, where I_N denotes the N-order identity matrix. Similarly, the signal received by the m-th communication user in the q-th slot can be written as:

$$\boldsymbol{y}_{c_m,q} = (\boldsymbol{S}_{m,q} + \boldsymbol{Z}_q)\,\boldsymbol{h}_{c_m,q} + \boldsymbol{n}_{c_m,q}, \tag{4}$$

where $\boldsymbol{h}_{c_m} \sim \mathcal{CN}(0, \boldsymbol{H}_{c_m})$ denotes the communication channel of the m-th user of the q-th time block, $\boldsymbol{n}_{c_m,q} \sim \mathcal{CN}(0, \boldsymbol{\Sigma}_{n_c})$ is the additive white Gaussian noise (AWGN) at the m-th communication receiver. $\boldsymbol{H}_{c_m}, \boldsymbol{\Sigma}_{n_c} \in \mathbb{R}^{N\times N}$ are the covariance matrices of the corresponding parametric distributions, $\boldsymbol{\Sigma}_{n_c} = \boldsymbol{I}_N \cdot \sigma_{n_c}^2$ because the noise samples are independent and identically distributed.

According to (4), the SINR of the received communication signal of the k-th channel in the q-th pulse $\gamma_q(k)$ can be written as:

$$\gamma_q(k) = \frac{|s_{m,q}(k)h_{c_m,q}(k)|^2}{|z_q(k)h_{c_m,q}(k)|^2 + \sigma_{n_c}^2}. \tag{5}$$

Since $h_{c_m,q}(k)$ is an independent one-dimensional complex Gaussian random variable with the variance $\sigma_{h_c}^2$, $|h_{c_m,q}(k)|^2$ follows the exponential distribution, $|s_{m,q}(k)|^2$ and $|z_q(k)|^2$ are the power distribution of the transmit waveforms which can be treated as invariants because they are fixed in the q-th time block. Thus the numerator and denominator in (5) also follow the exponential distribution. Then the probability density function (PDF) of the received SINR of the k-th communication channel in the q-th slot, $\Gamma_{q,k}(\gamma)$, can be written as:

$$\Gamma_{q,k}(\gamma) = \begin{cases} \dfrac{\mho(\gamma)\cdot\sigma_{n_c}^2 + 1}{|s_{m,q}(k)|^2|z_q(k)|^2\sigma_{h_c}^4\cdot\mho(\gamma)} \\ \qquad\qquad \times\exp\left(-\mho(\gamma)\cdot\sigma_{n_c}^2\right), & \gamma > 0, \\ 0, & \gamma \le 0. \end{cases} \tag{6}$$

where $\mho(\gamma) \triangleq \frac{\gamma}{|s_{m,q}(k)|^2\sigma_{h_c}^2} + \frac{1}{|z_q(k)|^2\sigma_{h_c}^2}$.

The outage probability with regarding to receiver threshold $\gamma_q^{th}(k)$ under the radar interference of transmit signal $z_q(k)$ can be calculated as:

$$\begin{aligned} P_{out-q}(\gamma_q^{th}(k); z_q(k)) &= \int_{-\infty}^{\gamma_q^{th}(k)} \Gamma_{q,k}(\gamma)\,\mathrm{d}\gamma \\ &= 1 - \frac{\exp\left(-\dfrac{\gamma_q^{th}(k)\cdot\sigma_{n_c}^2}{|s_{m,q}(k)|^2\sigma_{h_c}^2}\right)}{1 + \dfrac{\gamma_q^{th}(k)}{|s_{m,q}(k)|^2}|z_q(k)|^2}. \end{aligned} \tag{7}$$

By considering the impact of radar interference, we measure the communication AoI performance by using the transmission outage probability. The discrete AoI of the k-th channel of the q-th pulse can be obtained according to the AoI definition [24]: at the end of the q-th pulse in the channel, if the received SINR is larger than the receiver SINR threshold, then a successful transmission occurs, and the AoI at the qT moment equals T; If the packet fail to arrive the destination, the AoI at the qT moment equals the AoI of the last moment plus T. The possibility of a successful and failed transmission are $1 - P_{out-q}$ and P_{out-q} respectively. We assume that the channel condition and data transmission are independent in each channel, thus the outage of each channel are also independent.

$$A_q(k) \triangleq \begin{cases} A_{q-1}(k) + T, & \text{if } \gamma_q(k) < \gamma_q^{th}(k), \\ T, & \text{if } \gamma_q(k) \ge \gamma_q^{th}(k). \end{cases} \tag{8}$$

Theorem 1. The AoI expectation of the k-th channel in the q-th slot with regard to the real AoI of the $(q-1)$-th slot can be rewritten as:

$$\begin{aligned} E[A_q(k)|A_{q-1}(k)] = T + \left(1 - \frac{\exp\left(-\dfrac{\gamma_q^{th}(k)\cdot\sigma_{n_c}^2}{|s_{m,q}(k)|^2\sigma_{h_c}^2}\right)}{1 + \dfrac{\gamma_q^{th}(k)}{|s_{m,q}(k)|^2}|z_q(k)|^2}\right) \\ \times A_{q-1}(k) \triangleq \mathcal{A}_q(\gamma_q^{th}(k); z_q(k)). \end{aligned} \tag{9}$$

Proof. According to (8), $A_q(k)$ can be seen as a discrete random variable with two possible values when $A_{q-1}(k)$ is given, where $\mathrm{prob}(\gamma_q(k) < \gamma_q^{th}(k)) = P_{out-q}(\gamma_q^{th}(k); z_q(k))$. Thus the expectation of $A_q(k)$ with regard to $A_{q-1}(k)$ can be calculated as:

$$\begin{aligned} E[A_q(k)|A_{q-1}(k)] &= (A_{q-1}(k) + T)\cdot P_{out-q}(\gamma_q^{th}(k); z_q(k)) \\ &\quad + T\cdot(1 - P_{out-q}(\gamma_q^{th}(k); z_q(k))). \end{aligned} \tag{10}$$

Substituting $P_{out-q}(\gamma_q^{th}(k); z_q(k))$ in (7) into (10), (9) can be derived. ∎

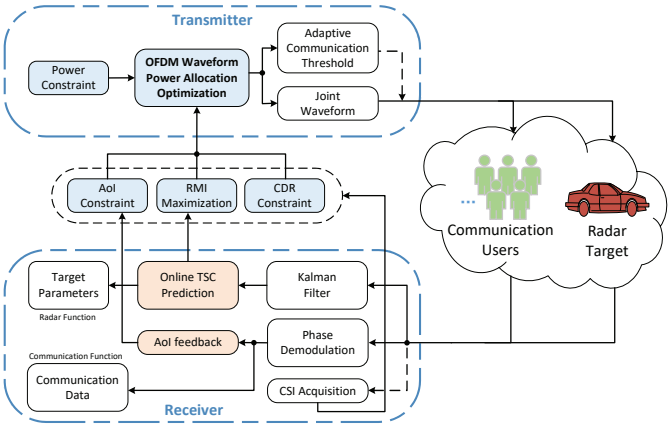

Fig. 2. The proposed cooperative waveform design framework of the JRC system.

According to (8), the AoI in each communication channel is a Markov process, the expectation of AoI in the k-th channel at the end of the qth slot can be calculated as:

$$\mathrm{E}[A_q(k)] = \frac{T}{1 - P_{out-q}(\gamma_q^{th}(k); z_q(k))} \tag{11}$$

It can be noticed that (11) is the expectation of AoI at a random moment with no prior information. Compared with conventional AoI expectation calculation of (11), which is obtained by the steady-state probabilities of the Markov chain, (10) is the expectation of the AoI at the q-th time block with the AoI of the past time block as the prior information, this value is only meaningful for the next moment, so it is a short-term indicator , updated in real time, which is more accurate than (11) for the reason of eliminating part of the uncertainty.

It is evident from (9) that the performance of the communication AoI provides more comprehensive information than the Shannon capacity. Although both values are directly influenced by the communication SINR, the AoI takes into account the practical factor of the receiver threshold in the transmission. Additionally, the AoI value emphasizes long-term performance by considering the outcome of previous transmissions. Therefore, by incorporating both the AoI and CDR value, the timeliness and rate of transmission can be jointly considered. According to (9), the achievable range of communication AoI of the k-th channel during the q-th pulse can be obtained by setting the radar signal to zero and maximum power respectively, which are given by (12), where p_k is the radar signal power upper bound of the k-th channel.

$$E[A_q(k)|A_{q-1}(k)]^{\min} = \mathcal{A}_q(\gamma_q^{th}(k); 0), \tag{12a}$$

$$E[A_q(k)|A_{q-1}(k)]^{\max} = \mathcal{A}_q(\gamma_q^{th}(k); p_k). \tag{12b}$$

III. Cooperative Framework Design and Problem Description

In this section, we first describe the cooperative waveform design framework of the JRC system to mitigate mutual interference, which features communication AoI feedback and online TSC prediction, as depicted in Fig. 2. We then discuss the optimization process for radar and communication functions individually. Finally, we formulate a non-convex optimization problem to achieve a satisfactory trade-off between the two functions.

A. Cooperative Framework Design

Fig. 2 shows our proposed cooperative waveform design framework of the JRC system. The proposed framework works as follows:

- In the transmitter, waveform optimization is conducted to improve radar and communication performance. After joint optimization, the optimal waveform power allocation result is obtained, and then the transmit signal is generated by the orthogonal waveform generator, with QPSK modulation conducted in the baseband. Adaptive communication threshold generated by the joint optimization block is embedded in the reference signal which is sent before data transmission, in order to notice the communication user in advance.
- In the receiver, the combined signal of the backscattered radar echo and the uplink communication signal is processed in two links to enable dual-function. The communication function processing link demodulates the received signal and then extracts communication information; the radar function processing link first extracts TSC from the received echo and then revises the predicted TSC value in order to obtain more accurate target parameter information.
- The cognition property of this framework is reflected in the signal processing loop: the TSC, AoI feedback, and CSI are extracted from the received signal, those information determine the objective function RMI and constraints AoI & CDR of the optimization problem, thereby affecting shaping transmitted waveform. Especially, in our proposed framework, communication AoI is considered as an important factor. According to (8), AoI can be modeled as a Markov chain, which makes the AoI feedback a crucial element in the signal processing loop.
- As for channel state information (CSI), before optimizing and transmitting each waveform, a CSI matrix is estimated for this pulse at both UE (downlink) and BS (uplink) sides to support communication services. Specifically, predefined symbols are transmitted. When the symbol signal arrives at the receiver, CSI is estimated by comparing the received signal with the known transmitted signal. CSI matrix can be measured using synchronization signal block (SSB) and reference signal such as demodulation reference signal (DMRS) [32], [33]. The signal processing link at this time is marked by dashed lines in Fig. 2.

B. AoI-aware Waveform Optimization for the Radar Function

The radar function require high mutual information to achieve accurate target recognition, thus we optimize radar waveform for RMI maximization. Compared with the previous work [21] and [22], since we consider an additional communication constraint of AoI in designing radar waveform,

the radar sub-system will inevitably lose a part of its own performance under the same power constraint as a price. This is essentially due to the addition of constraint, which cannot be eliminated under the same optimization model. For the benefit of radar's optimal functioning, we introduce Kalman filter (KF)-based cognitive signal processing to solve this problem by accumulating long-term experience and revising TSC prediction value in an online way.

1) Offline TSC Prediction: Without considering the temporal correlation between radar echoes, radar receiver uses MAP method to estimate the TSC of the target traditionally, the MAP algorithm can be expressed as [34]:

$$\widehat{\boldsymbol{g}}_{r,q} = \arg\max_{\boldsymbol{g}_{r,q}} \text{prob}(\boldsymbol{g}_{r,q}|\boldsymbol{y}_{r,q}) = \boldsymbol{D}_q \boldsymbol{y}_{r,q}, \tag{13}$$

where $\text{prob}(\bullet)$ denotes the conditional probability distribution of $\boldsymbol{g}_{r,q}$ given the received signal $\boldsymbol{y}_{r,q}$,

let $\boldsymbol{Z}_q^S \triangleq \boldsymbol{Z}_q + \sum_{m=1}^{M} \boldsymbol{S}_{m,q}$, then the MAP filter $\boldsymbol{D}_q$ can be defined as:

$$\boldsymbol{D}_q = \left({\boldsymbol{Z}_q^S}^H \boldsymbol{\Sigma}_{n_r}^{-1} \boldsymbol{Z}_q^S + \boldsymbol{G}_r^{-1} \right)^{-1} {\boldsymbol{Z}_q^S}^H \boldsymbol{\Sigma}_{n_r}^{-1}. \tag{14}$$

Then the estimation error can be obtained by $\epsilon_{MAP-q} = \frac{1}{N}\text{tr}(\boldsymbol{P}_{MAP-q})$, where $\text{tr}(\bullet)$ denotes the trace of a matrix, $\boldsymbol{P}_{MAP_q}$ is the mean square error (MSE) matrix of MAP-based estimation method, which can obtained by:

$$\begin{aligned} \boldsymbol{P}_{MAP-q} &= \varepsilon\{(\widehat{\boldsymbol{g}}_{r,q} - \boldsymbol{g}_{r,q})(\widehat{\boldsymbol{g}}_{r,q} - \boldsymbol{g}_{r,q})^H\} \\ &= \boldsymbol{D}_q(\boldsymbol{Z}_q^S \boldsymbol{G}_r {\boldsymbol{Z}_q^S}^H + \boldsymbol{\Sigma}_{n_r})\boldsymbol{D}_q^H \\ &\quad -\boldsymbol{D}_q \boldsymbol{Z}_q^S \boldsymbol{G}_r - \boldsymbol{G}_r {\boldsymbol{Z}_q^S}^H \boldsymbol{D}_q^H + \boldsymbol{G}_r. \end{aligned} \tag{15}$$

2) Online TSC Prediction: Taking the correlation between the TSCs estimated by nearby radar echoes into consideration, a KF-based method is adopted in this paper for online prediction by revising estimation errors in a closed loop through previous observations combined with the predicted value. (16) is an exponential correlated model between TSCs at different times which is derived according to real radar data [35], [36]:

$$\boldsymbol{g}_{r,q} = e^{-\frac{T}{\tau}} \boldsymbol{g}_{r,q-1} + \boldsymbol{u}_{q-1}, \tag{16}$$

where τ denotes the temporal decay constant describing the temporal TSC correlation between two neighboring echoes, $\boldsymbol{u}_{q-1}$ the excitation noise vector with zero mean and covariance matrix $(1 - e^{-\frac{2T}{\tau}})\boldsymbol{G}_r$.

According to (3) and (13-16), the online TSC prediction equations conducted by the Kalman filter recursion can be expressed as follows [37]:

State prediction:

$$\widehat{\boldsymbol{g}}_{r,q|q-1} = e^{-T/\tau} \boldsymbol{g}_{r,q-1|q-1}. \tag{17}$$

Covariance matrix of prediction:

$$\boldsymbol{P}_{q|q-1} = e^{-2T/\tau} \boldsymbol{P}_{r,q-1|q-1} + (1 - e^{-2T/\tau})\boldsymbol{G}_r. \tag{18}$$

Kalman gain:

$$\boldsymbol{K}_q \triangleq \boldsymbol{P}_{q|q-1} {\boldsymbol{Z}_{m,q}^S}^H (\boldsymbol{D}_q \boldsymbol{\Sigma}_{n_r} + \boldsymbol{D}_q \boldsymbol{Z}_{m,q}^S \boldsymbol{P}_{k|k-1} {\boldsymbol{Z}_{m,q}^S}^H)^{-1}. \tag{19}$$

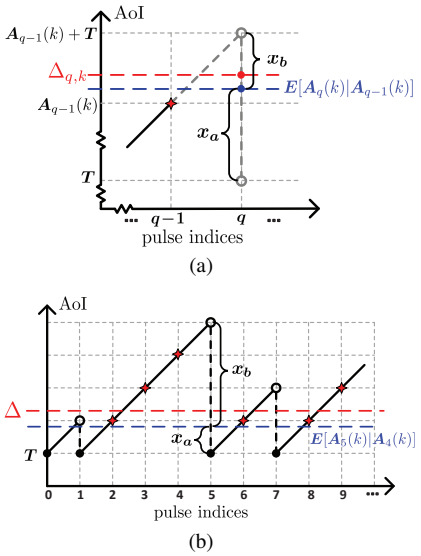

Fig. 3. Graphic explanation of the AoI-aware waveform optimization principle.

State estimation:

$$\widehat{\boldsymbol{g}}_{r,q|q} = \widehat{\boldsymbol{g}}_{r,q|q-1} + \boldsymbol{K}_q(\widehat{\boldsymbol{g}}_{r,q} - \boldsymbol{D}_q \boldsymbol{Z}_{m,q}^S \widehat{\boldsymbol{g}}_{r,q|q-1}). \tag{20}$$

Covariance matrix of estimation:

$$\boldsymbol{P}_{q|q} = \boldsymbol{P}_{q|q-1} - \boldsymbol{K}_q \boldsymbol{D}_q {\boldsymbol{Z}_{m,q}^S}^H \boldsymbol{P}_{q|q-1}. \tag{21}$$

Thus the estimation error of the q-th iteration can be expressed as: $\epsilon_{KF-q} = \frac{1}{N} tr(\boldsymbol{P}_{q|q})$.

3) Waveform optimization principles: We aim to achieve better RMI by optimizing radar waveform as well as mitigating the interference to communication users. According to (3), the estimated RMI between the radar received signal and the target echo with regard to the transmit signal $\boldsymbol{z}_q$ can be written as [18]:

$$\begin{aligned} \mathcal{I}_q &= I(\boldsymbol{g}_{r,q}; \boldsymbol{y}_{r,q}|\boldsymbol{z}_q) \\ &= \sum_{k=1}^{N} \log \left(1 + \frac{\left| z_q(k) \widehat{g}_{r,q|q-1}(k) \right|^2}{\sum_{m=1}^{M} \sum_{k \in \mathbb{K}_m} \left| s_{m,q}(k) \widehat{g}_{r,q|q-1}(k) \right|^2 + \sigma_{n_r}^2} \right). \end{aligned} \tag{22}$$

According to (7), radar signal affect communication outage by adding interference to communication channel, which will reflect on the AoI of the communication users, thus we adjust radar signal to manage this interference. For a fixed $\gamma_q^{th}(k)$, (9) can be seen as a function only related to $z_q(k)$. As shown by Fig. 3 (a), for the k-th channel of the q-th pulse, assuming each communication user only occupies one channel, we set an AoI expectation bound $\Delta_{q,k}$, then $E[A_q(k)|A_{q-1}(k)] \leq \Delta_{q,k}$ should be hold for all k. For communication users that occupy multiple channels, we set an AoI expectation bound $\Delta_q^m = \frac{1}{N_m} \sum_{k \in \mathbb{K}_m} \Delta_{q,k}$ for each user, then $\frac{1}{N_m} \sum_{k \in \mathbb{K}_m} E[A_q(k)|A_{q-1}(k)] \leq \Delta_q^m$ should be hold for all m. This constraint will be triggered to be active whenever the AoI value of next pulse has an opportunity to

across the AoI expectation bound. Assuming $\Delta_{q,k} = \Delta, \forall q, k$, Fig. 3 (b) shows a possible communication AoI curve, where the pulses that the AoI constraint should be active is marked by red stars. Also, communication channel capacity is considered as $\sum_{k\in\mathbb{K}_m} \log(1+\gamma_q(k)) \geq \chi_{m,q}$ for all m.

Lemma 1. The ratio of the two AoI value margins, indicated as x_a and x_b in Fig. 3, is related to the communication outage probability, which can be expressed as follows:

$$\frac{x_a}{x_b} = \frac{p_{out-q}(\gamma_q^{th}(k); z_q(k))}{1 - p_{out-q}(\gamma_q^{th}(k); z_q(k))} \tag{23}$$

Proof. It can be easily obtained from Fig. 3 that $x_a = E[A_q(k)|A_{q-1}(k)] - T$ and $x_b = A_{q-1}(k) + T - E[A_q(k)|A_{q-1}(k)]$. According to (10), they can be further expressed as: $x_a = A_{q-1}(k) \cdot p_{out-q}(\gamma_q^{th}(k); z_q(k))$ and $x_b = A_{q-1}(k) \cdot [1 - p_{out-q}(\gamma_q^{th}(k); z_q(k))]$, thus the result of (23) is obvious. ■

According to (8), the AoI value is generated through a binary decision, an extremely high value of SINR $\gamma_q(k)$ or a significant suppression of radar function waveform power do not meaningfully enhance AoI performance, contrasting with the case of CDR. As illustrated in Fig. 3, to attain a lower average AoI, we should focus on channels with poor conditions to prevent AoI escalation. Consequently, if the optimization of power distribution indicates allocating more power into less interfered channel, it could worsen the AoI performance: poorly connected channels are neglected and allocated with minimal power, leading to increasing AoI values in these channels.

According to *Lemma* 1, the proposed waveform optimization principle manages to achieve AoI-awareness through the following process: by optimizing the radar waveform $z_q(k)$ and communication threshold $\gamma_q^{th}(k)$, we control the outage probability of the corresponding communication link, which helps to move the AoI expectation level of the next pulse (which is marked by the blue dashed line in Fig. 3) down the required value (which is marked by the red dashed line in Fig. 3). Therefore, as can be seen from Fig. 3(b), the larger $A_{q-1}(k)$ is, the smaller the ratio x_a/x_b should be, which indicates a smaller outage probability and more severe suppression on radar interference.

C. Adaptive Threshold Adjustment for the Communication Function

For a fixed radar interference $z_q(k)$, we redefine a function that only treats the receiver threshold as a variable, which is expressed as follows:

$$f_{q,k}^{th}(\gamma) \triangleq \mathcal{A}_q(\gamma; z_q(k)) = T + \left(1 - \frac{\exp(-\rho_1\gamma)}{1+\rho_2\gamma}\right) A_{q-1}(k). \tag{24}$$

where $\rho_1 = \frac{\sigma_{n_c}^2}{|s_{m,q}(k)|^2\sigma_{h_c}^2}$, $\rho_2 = \frac{|z_q(k)|^2}{|s_{m,q}(k)|^2}$ are related to radar waveform, communication signal, communication channel conditions, and system noise.

Given a certain AoI constraint value for the k-th communication channel, we set the communication receiver threshold of the k-th channel according to the following expression:

$$(C1) \quad \gamma_q^{th}(k) = \min\{\gamma_u, \max\{\gamma_l, \tilde{f}_{q,k}^{th\ -1}(\Delta_{q,k})\}\}, \tag{25}$$

where γ_l is the minimal SINR level demanded by the communication receiver which guarantees subsequent signal processing, γ_u is the SINR threshold upper limit corresponding to the maximum acceptable AoI, $\Delta_{q,k}$ is a preset AoI constraint value for the k-th communication channel in the q-th time block. $\tilde{f}_{q,k}^{th\ -1}(\cdot)$ stands for the extended-value extension of the inverse function of (24), see Appendix A for more details.

Lemma 2. (25) is a monotone non-decreasing function.

Proof. Please refer to the Appendix. ■

Note that according to *Lemma* 3, at a certain pulse where the transmitted communication information and the communication channel conditions as well as system noise are estimated, given a value of AoI constraint, there will be only one threshold setting corresponding to a fixed radar power allocation scheme.

D. Problem Description

The optimization goal in this paper is to maximize RMI subjected to the threshold adjustment constraints $(C1)$, the radar sum transmit power constraint $(C2)$, the power upper bound for single channel $(C3)$, the communication sum capacity constraints $(C4)$, and the communication average AoI constraints $(C5)$. The joint optimization problem can be expressed as:

$$\begin{aligned}
(P1) \quad & \max_{\boldsymbol{z_q}, \boldsymbol{\gamma_q^{th}}} \quad \mathcal{I}_q \\
& s.t. \quad (C1) \\
& (C2) \ \sum_{k=1}^{N} |z_q(k)|^2 \leq \mathrm{P_r}, \\
& (C3) \ |z_q(k)|^2 \leq p_k, \quad \forall k \in \mathbb{N}, \\
& (C4) \ \sum_{k\in\mathbb{K}_m} \log(1+\gamma_q(k)) \geq \chi_q^m, \quad \forall m \in \mathbb{M}, \\
& (C5) \ \frac{1}{N_m} \sum_{k\in\mathbb{K}_m} E[A_q(k)|A_{q-1}(k)] \leq \Delta_q^m, \quad \forall m \in \mathbb{M},
\end{aligned} \tag{26}$$

where χ_q^m denotes the sum capacity constraint of the m-th user, $\mathbb{M} = \{1, 2, 3, \cdots, M\}$ is the index set of the communication users. The power upper bound for each channel $(C3)$ is considered in order to mitigate the inherent weakness of OFDM signal by limiting the subcarrier power ratio (SPR) [38], [39], to avoid the situation that the transmitter works in the nonlinear region of power amplifier. p_k satisfies $|z_q(k)|^2/(\sum_{k=1}^{N}|z_q(k)|^2) \leq p_k/P_r$.

There are two main differences between constraint $(C4)$ and $(C5)$: 1) In terms of its physical interpretation, $(C4)$ focus on the instantaneous data rate, which is obtained by Shannon's capacity formula, so $(C4)$ depicts the highest error-free data rate this communication system can achieve. While $(C5)$ focus on the data freshness, which counts the whole time

period since the data was generated till it was received, so $(C5)$ depicts whether the transmission status is successful or failed. 2) In terms of mathematical calculation, $(C4)$ is only influenced by the communication SINR, theoretically if the interference-plus-noise level can be controlled low enough, the CDR can be raised up to any high value. While $(C5)$ is related not only to the SINR, but also the past AoI and the receiver SINR threshold, so $(C5)$ needs more information at each moment to obtain its value. Moreover, under a certain setting of the last AoI value A_{q-1} and the receiver SINR threshold γ_q^{th}, there exists a one-to-one correspondence between the AoI and CDR constraints.

According to [22], each constraint of $(C4)$ is a non-convex set. Similarly, constraints in $(C5)$ are also non-convex, thus $(P1)$ is a multi-variable optimization problem with 2M non-convex constraints, which can not be solved directly.

IV. The proposed CS-CD Method

This section introduces the procedure of our proposed method to construct and solve the optimization problem $(P1)$. Since $(P1)$ is a hard non-convex problem and can not be solved directly, we propose a constraints-splitting coordinate descent (CS-CD) method, which is based on the coordinate descent method but we splits the non-convex constraints using the output of the last round and convert them into multiple convex ones at each iteration, then solve the original problem iteratively. The whole course can be divided into 3 steps, conducting the mathematical simplification, problem transformation, and algorithms, respectively.

A. Mathematical Simplification

Let $w(k) = |z_q(k)|^2$, $\tilde{\gamma}(k) = \gamma_q^{th}(k)$, $\varphi_k = \frac{\left|\widehat{g}_{r,q|q-1}(k)\right|^2}{|s_{m,q}(k)|^2\left|\widehat{g}_{r,q|q-1}(k)\right|^2+\sigma_{n_r}^2}$, $p_1(k) = \mathrm{p_k}$, $\lambda_{1k} = \frac{1}{|s_{m,q}(k)|^2}$, $\lambda_{2k} = \frac{\sigma_{n_c}^2}{|s_{m,q}(k)|^2\cdot|h_{cm,q}(k)|^2}$, $a_k = -\frac{\sigma_{n_c}^2}{|s_{m,q}(k)|^2\sigma_{h_c}^2}$, $b_k = \frac{1}{|s_{m,q}(k)|^2}$, $(P1)$ can be equivalently simplified into the following form:

$$\begin{aligned}
(P2)\quad \max_{\boldsymbol{w},\tilde{\boldsymbol{\gamma}}}\quad & \sum_{k=1}^{N}\log(1+\varphi_k w(k)) \\
s.t.\quad & (C1), \\
& (C6)\ \mathbf{1}^{\boldsymbol{T}}\boldsymbol{w} \le \mathrm{P_r}, \\
& (C7)\ \mathbf{0} \preceq \boldsymbol{w} \preceq \boldsymbol{p_1}, \\
& (C8)\ \sum_{k\in\mathbb{K}_m}\log\left(1+\frac{1}{\lambda_{1k}w(k)+\lambda_{2k}}\right) \\
& \qquad \ge \chi_{m,q}, \qquad \forall m\in\mathbb{M}, \\
& (C9)\ \sum_{k\in\mathbb{K}_m}\left[T+\left(1-\frac{\exp(a_k\tilde{\gamma}(k))}{1+b_k\tilde{\gamma}(k)w(k)}\right)\right. \\
& \qquad \left.\times A_{q-1}(k)\right] \le N_m\Delta_q^m, \quad \forall k\in\mathbb{N},
\end{aligned} \tag{27}$$

where $(C2)$, $(C3)$, $(C4)$, $(C5)$ are equivalently transformed into $(C6)$, $(C7)$, $(C8)$, $(C9)$, respectively.

B. Problem Transformation

While the property of not convex of $(P2)$ is essentially due to the constraints of $(C8)$ and $(C9)$, in which each communication constraint of the m-th user is shared by N_m channels that the user occupied. We split the sum constraints of the m-th user into N_m shares and assign them to all its channels. Any allocation scheme will correspond to a new optimization problem with $2N+3$ constraints, and the optimal solution of each new problem represents a possible solution of problem $(P2)$, the optimal solution of $(P2)$ must corresponds to one of these schemes.

Therefore, by splitting the sum constraint of $(C8)$ into single constraints and assign them to each channel, $(C8)$ can be transformed into the following expression:

$$\log\left(1+\frac{1}{\lambda_{1k}w(k)+\lambda_{2k}}\right) \ge \delta_k\chi_{m,q}, \quad \forall k\in\mathbb{K}_m, m\in\mathbb{M}, \tag{28}$$

where δ_k is the proportion borne by the k-th channel of the m-th user, which can be expressed as (29) and is determined through iteration.

$$\delta_k \triangleq \frac{\log\left(1+\frac{1}{\lambda_{1k}w(k)+\lambda_{2k}}\right)}{\sum_{\tilde{k}\in\mathbb{K}_m}\log\left(1+\frac{1}{\lambda_{1\tilde{k}}w(\tilde{k})+\lambda_{2\tilde{k}}}\right)}. \tag{29}$$

Hence, (28) can be further expressed as:

$$\begin{aligned}
(C10)\quad w(k) \le \frac{1}{\lambda_{1k}}\left(\frac{1}{2^{\delta_k\chi_{m,q}}-1}-\lambda_{2k}\right) \triangleq p_2(k), \\
\forall k\in\mathbb{K}_m, m\in\mathbb{M}.
\end{aligned} \tag{30}$$

Similarly, by splitting the sum constraint of $(C9)$ into single constraints and assign them to each channel, $(C9)$ can be transformed into the following expression:

$$\begin{aligned}
(C11)\quad & T+\left(1-\frac{\exp(a_k\tilde{\gamma}(k))}{1+b_k\tilde{\gamma}(k)w(k)}\right)A_{q-1}(k) \\
& \le \xi_k N_m\Delta_q^m, \quad \forall k\in\mathbb{K}_m, m\in\mathbb{M},
\end{aligned} \tag{31}$$

where ξ_k is the proportion borne by the k-th channel of the m-th user , which can be expressed as (32) and is determined through iteration.

$$\xi_k \triangleq \frac{T+\left(1-\frac{\exp(a_k\tilde{\gamma}(k))}{1+b_k\tilde{\gamma}(k)w_k}\right)A_{q-1}(k)}{N_mT+\sum_{\tilde{k}\in\mathbb{K}_m}\left(1-\frac{\exp(a_k\tilde{\gamma}(\tilde{k}))}{1+b_{\tilde{k}}\tilde{\gamma}(\tilde{k})w_{\tilde{k}}}\right)A_{q-1}(\tilde{k})}. \tag{32}$$

Therefore, a sum-constraints-splitting optimization problem is generated, which can be written as:

$$\begin{aligned}
(P3)\quad \max_{\boldsymbol{w},\tilde{\boldsymbol{\gamma}}}\quad & \sum_{k=1}^{N}\log(1+\varphi_k w(k)), \\
s.t.\quad & (C1),\ (C6),\ (C7),\ (C10),\ (C11).
\end{aligned} \tag{33}$$

According to *Lemma* 3, for a fixed $w(k)$, there is one precise $\tilde{\gamma}(k)$ corresponding to the AoI constraint weight ξ_k, thus $\tilde{\boldsymbol{\gamma}}$

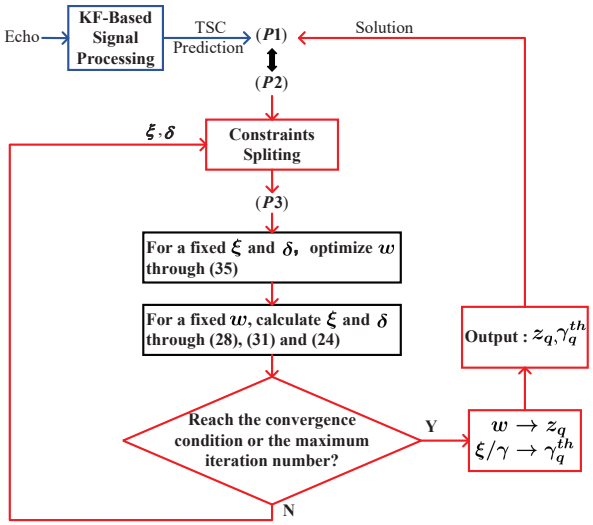

Fig. 4. Flow diagram of the CS-CD method.

can be represented by $\boldsymbol{\xi}$. Combining (25) with (31), $(C1)$ and $(C11)$ can be jointly represented as:

$$(C12)\quad w(k) \le \left(\frac{\exp(a_k\tilde{\gamma}_k')}{1-\min\left(1_-,\frac{\xi_k N_m \Delta_q^m - T}{A_{q-1}(k)}\right)}-1\right)\frac{1}{b_k\tilde{\gamma}_k'} \triangleq p_3(k), \qquad \forall k\in\mathbb{K}_m, m\in\mathbb{M}, \tag{34}$$

where $\tilde{\gamma}_k' = \min\{\gamma_u, \max\{\gamma_l, \tilde{f}_{q,k}^{th\ -1}(\xi_k N_m \Delta_q^m)\}\}$, 1_- represents the left limit of 1, infinitely close to the value of 1 but always less than 1. This is to prevent a situation of $\frac{\xi_k N_m \Delta_q^m - T}{AoI_{q-1}(k)} \ge 1$ under good channel conditions, where $(C11)$ should be set as inactive.

For a fixed $\boldsymbol{\xi}$, It is noticeable that $(C9)$, $(C10)$, $(C12)$ are all linear constraints with the same form, combining these three constraints with $\tilde{p}_k = \min\{p_1(k), p_2(k), p_3(k)\}$, we have:

$$\begin{aligned}(P4)\quad \max_{\boldsymbol{w}}\quad & \sum_{k=1}^{N}\log(1+\varphi_k w(k)),\\ s.t.\quad & (C6),\\ & (C13)\quad \mathbf{0}\preceq \boldsymbol{w}\preceq\tilde{\boldsymbol{p}},\quad \forall k\in\mathbb{K}_m, m\in\mathbb{M},\end{aligned} \tag{35}$$

$(P4)$ is a classic convex problem with a positive convex objective function and several linear constraints. Exploiting the Lagrange multiplier method, the optimal solution of $(P4)$ can be obtained by solving the KKT condition, which is given in (36) [40].

$$w^*(k) = \begin{cases} 0, & \frac{1}{v^*} \le \frac{1}{\varphi_k},\\ \tilde{p}_k, & \frac{1}{v^*} \ge \frac{1}{\varphi_k} + \tilde{p}_k,\\ \frac{1}{v^*} - \frac{1}{\varphi_k}, & \frac{1}{\varphi_k} \le \frac{1}{v^*} \le \frac{1}{\varphi_k} + \tilde{p}_k. \end{cases} \tag{36}$$

where v^* is the Lagrange multiplier of the constraint $(C8)$.

For a fixed $\boldsymbol{w}$, $\boldsymbol{\delta}$ can be obtained through (29), and $\boldsymbol{\xi}$ can be obtained by simultaneously set equations (25) and (32).

Algorithm 1 KF-Based Method for Setting TSC Parameter of $(P1)$

Input: Total pulse number Q, communication data $\boldsymbol{o}_{m,q}$, $\forall m, q$.

1: **Initialization:** $\boldsymbol{y}_{r,1} \leftarrow$ (3), $\hat{\boldsymbol{g}}_{r,1} \leftarrow$ (13), $\boldsymbol{P}_{1|1} \leftarrow$ (15), $\boldsymbol{\gamma}_1 \leftarrow$ (5), $A_1^m \leftarrow$ (8), set a random initial waveform $\boldsymbol{z}_1$.
2: **for** $q = 2$ to Q **do**
3: **Prediction:** $\hat{\boldsymbol{g}}_{r,q|q-1} \leftarrow$ (17).
4: **Covariance matrix of prediction** : $\boldsymbol{P}_{q|q-1} \leftarrow$ (18).
5: **Optimization:** optimize $\boldsymbol{z}_q$ and $\tilde{\boldsymbol{\gamma}}_q^{th}$ through Algorithm 2 with regard to $\hat{\boldsymbol{g}}_{r,q|q-1}$ and A_{q-1}^m.
6: **Transmit, Receive and Record**: Transmit optimized radar waveform $\boldsymbol{z}_q$, receive radar echo $\boldsymbol{y}_{r,q}$ and communication users' feedback A_q^m.
7: **Measure:** $\hat{\boldsymbol{g}}_{r,q} \leftarrow$ (13).
8: **Kalman gain:** $\boldsymbol{K}_q \leftarrow$ (19).
9: **Estimation:** $\hat{\boldsymbol{g}}_{r,q|q} \leftarrow$ (20).
10: **Covariance matrix of estimation** : $\boldsymbol{P}_{q|q} \leftarrow$ (21).
11: **end for**

C. Algorithms

Finally, we develop a series of algorithms which exploit the key transformation procedure mentioned above to solve the initial problem at hand. Fig. 4 shows the flow diagram of this process, which is elaborated below.

1) KF-Based Signal Processing for TSC Prediction: As shown by the blue part in Fig. 4, the first algorithm conducts the TSC estimation and helps construct the objective function in (26) for further system optimization, which is described in Algorithm 1. It features *Prediction*, *Measure*, and *Estimation* steps, which are essential in the Kalman filter and has been calculated in Section III. The process will be repeated Q times, generating a TSC prediction at each time, which is a key parameter for further optimization.

Note that we do not execute the optimization procedure after the estimation of $\hat{\boldsymbol{g}}_{r,q|q}$, instead, we use the prediction value of $\hat{\boldsymbol{g}}_{r,q|q-1}$, which is more instructive and meaningful.

2) Constraint Splitting and Iterative Solving: As shown by the red part in Fig. 4, the most critical segment in CS-CD is conducted by Algorithm 2. To be started, it requires an input of a convergence coefficient η and a maximum number of iterations I_{max} to define a condition to break out of the loop. This algorithm works as follows. Firstly, we exploit the mathematical simplification to convert $(P1)$ equivalently into $(P2)$, then we split the sum constraints of $(P2)$ with the weights of $\boldsymbol{\delta}$ and $\boldsymbol{\xi}$ which have been initialized and will be recalculated during each iteration, thus $(P3)$ is generated. By fixing $\boldsymbol{\delta}$ and $\boldsymbol{\xi}$ to the value generated by last round, we convert $(P3)$ into a single-variable convex optimization problem, $(P4)$. Solving $(P4)$ to get an optimized $\boldsymbol{w}$, then for this certain $\boldsymbol{w}$, we calculate $\tilde{\boldsymbol{\gamma}}$ and the weights $\boldsymbol{\delta}$ and $\boldsymbol{\xi}$ for the next round, then we split $(P2)$ using the new weights, until reaching the convergence condition of the algorithm or the maximum iteration round number.

Algorithm 2 Constraint Splitting and Iterative Solving of $(P1)$

Input: $\eta > 0$, $I_{max} \in \mathrm{R}^{+}$.
Output: $\boldsymbol{z}_q$, $\tilde{\boldsymbol{\gamma}}_q^{th}$.

Initialization: $i = 0$, $\boldsymbol{w^0} = P_r/N$.
repeat
  $i = i + 1$.
  $\tilde{\boldsymbol{\gamma}}_q = \boldsymbol{\gamma}_q^{th} \leftarrow (25)$, $\delta_k^i \leftarrow (29)$, $\xi_k^i \leftarrow (32)$, with respect to $\boldsymbol{w^{i-1}}$.
  Split $(P2)$ by δ_k^i and ξ_k^i, obtain $(P3)$.
  Fix $\tilde{\boldsymbol{\gamma}}_{\boldsymbol{q}}$, obtain $(P4)$.
  Get $\boldsymbol{w^i}$ by solving $(P4)$ through (36).
  Calculate $\mathcal{I}_q^i$ through (22).
until $\left|\mathcal{I}_q^i - \mathcal{I}_q^{i-1}\right| \leq \eta \mathcal{I}_q^{i-1}$ or $i \geq I_{max}$.
Set $\delta_k^* = \delta_k^i$, $\xi_k^* = \xi_k^i$.
$\tilde{\gamma}_q(k) \leftarrow (25)$, with regard to ξ_k^* .
$z_q(k) = \sqrt{w^i(k)} \cdot \arg\{o_{m,q}(k)\}$, $\gamma_q^{th}(k) = \tilde{\gamma}_q(k)$.
return $\boldsymbol{z_q}$, $\boldsymbol{\gamma_q^{th}}$.

TABLE I
SIMULATION SETTING

Parameter		
Notation	**Description**	**Value**
Q	Number of pulses	**512**
N	Number of channels	**50**
M	Number of communication users	**10**
$\mathrm{P_r}$	Total transmit power of radar-purpose waveform	**10W**
$\mathrm{P_c}$	Total transmit power of communication-purpose waveform	**5W**
γ_u	Upper bound of the communication receiver threshold	**$-$11dB**
γ_l	Lower bound of the communication receiver threshold	**$-$25dB**
σ_{n_c}	Noise variance of communication receiver signal processing	**1**
σ_{n_r}	Noise variance of radar receiver signal processing	**1**
σ_{h_c}	Communication channel gain	**1**
σ_{g_r}	Covariance of TSC samples	**5**
T	Pulse duration	**1ms**
τ	Temporal decay constant	**1s**
χ	Communication capacity requirement	**0.077 bit/s**
Δ	AoI expectation bound of each user	**3T**

V. SIMULATION RESULTS

In this section, numerical results demonstrate the efficacy of our proposed method and evaluate the performance of the proposed algorithms through simulation. This section comprises two subsections, which evaluate the proposed cooperative waveform design framework and the AoI-aware oneline prediction optimization scheme, respectively. The parameter settings for our simulations can be found in Table I.

We consider $Q = 512$ consecutive pulses, the transmit waveform and the communication threshold are optimized in advance at each pulse and then embedded into the subsequent pulse. The optimization process is conducted Q times and we record the real RMI, CDR, and AoI at each pulse to analyze the performance of different schemes. A larger RMI value indicates that more target information can be extracted from the radar echo, and a smaller AoI value indicates that fresher data can be received by the communication users.

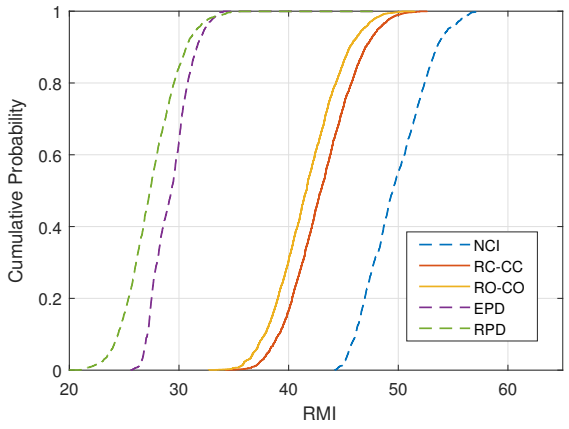

Fig. 5. Cumulative probability of RMI value of different waveforms.

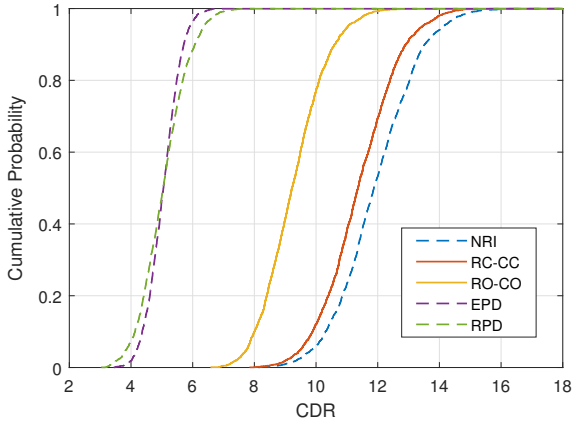

Fig. 6. Cumulative probability of CDR value of different waveforms.

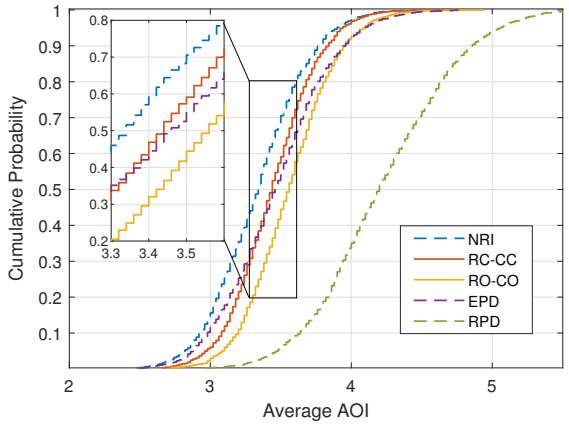

Fig. 7. Cumulative probability of AoI value of different waveforms.

A. Cooperative Waveform Design Framework

In the first subsection, we compare the waveform designed by our proposed cognitive framework with four benchmark waveforms in terms of the the RMI, CDR, and AoI performance. The proposed and benchmark waveforms are recognized by

- **NCI / NRI**: No Communication Interference / No Radar Interference. (A single waveform operating either radar or communication function).
- **RC-CC**: Radar-Centric Communication-Constrained waveform. (With cooperative interference control: proposed)
- **RO-CO**: Radar-Optimal plus Communication-Optimal waveform. (Optimized separately and with no cooperative interference control)
- **EPD**: Even power distribution waveform.
- **RPD**: Random power distribution waveform.

Fig. 5-7 shows the experimental cumulative distribution functions (CDFs) of the RMI, CDR, and AoI value of $Q = 512$ consecutive pulses. The figures have the RMI, CDR, or AoI value represented on the horizontal axis, while the vertical axis denotes the cumulative probability of the experimental value being less than or equal to the corresponding value on the horizontal axis. A closer proximity of the AoI curve to the Y-axis or a greater distance of the CDR curve from the Y-axis indicates better communication performance, and a greater distance of the MI curve from the Y-axis indicates better radar sensing performance. We highlight the RC-CC and RO-CO schemes, characterized by solid lines in the figures, in contrast to other benchmark schemes denoted by dashed lines.

As shown in Fig. 5-7, it is evident that radar and communication cause interference to each other, which is why the NRI / NCI waveform outperforms the other four waveforms in all the three metrics. If there is no waveform optimization in the system, such as adopting the EPD or RPD waveform, then a serious deterioration in both RMI and CDR performance will be observed. If we optimize radar and communication function waveform separately, the radar and communication performance loss can be improved significantly. However, although waveform optimization is conducted, there is still a big performance gap from the interference-free situation, this unsatisfactory performance is due to the the lack of cooperation between radar and communication. Compared with the RO-CO waveform, our proposed RC-CC waveform manages to achieve additional performance improvements by sharing waveform power distribution between the radar and communication functions which helps to obtain additional knowledge of the mutual interference. A better decision of waveform power allocation can be made to utilize the system power resource more efficiently.

According to Fig. 5-7, it is noticeable that the RC-CC waveform improves the RMI, CDR, and AoI performance to different degrees. This is because our proposed cognitive framework which generates the RC-CC waveform consider communication as the prime function and radar sensing as the secondary function, the principle of waveform design in this framework is to make the prime function's performance guaranteed and the secondary function's performance as good as possible, so within the limited power budget, the CDR performance gets more improvements rather than the RMI. As can be seen in Fig. 6, the CDR performance of the RC-CC waveform is very close to the NRI waveform which is the interference-free situation. As a cost, the secondary radar function improvement is not as significant, but the RC-CC waveform still outperforms the RO-CO waveform in terms of the RMI performance.

In Fig. 7, the comparison of AoI performance reveals a distinct phenomenon, where the RPD waveform shows an extremely poor performance while the EPD waveform is even better than the RO-CO waveform. This can be attributed to the unique feature of the AoI definition. According to 8, the AoI value is generated through a binary decision, an extremely high value of SINR $\gamma_q(k)$ or a great suppression of radar function waveform power is meaningless for improving the AoI performance, which is very different with the case of CDR. As can be seen from Fig. 3, to achieve a lower average AoI, we should just pay attention to the poor-connected channels and prevent the escalation of the AoI value. With this explanation, it is obvious that the RPD waveform shows the worst AoI performance, because if the poor-connected channels were randomly allocated with a low power value, the AoI value of this channel would continue to climb, and raise the average level of the AoI value. In contrast, the EPD waveform spread power over all the channels, which will avoid excessive AoI value of each single channel. The RO-CO waveform has poorer AoI performance than the EPD waveform, because the optimization of power distribution indicates allocating more power into less interfered channel, this will cause a dire situation in terms of the AoI performance: poor-connected channel was despised and being allocated with little power, which then leads to mounting AoI value in poor channels. However, the AoI performance can still be improved without discarding the waveform power optimization. By adopting our proposed cooperative framework, the RC-CC waveform manage to decrease the average AoI by exploiting additional knowledge of the radar-communication interference.

B. AoI-aware Online Prediction Waveform Power Distribution Optimization

Subsequently, to further explore the impact of the introduced AoI constraint and the online prediction procedure in the superior **RC-CC** waveform design framework, we alter the constraint in the optimization and compare the AoI and RMI performance of the following 3 benchmark schemes:

- **A-OnP**: AoI-aware Online Prediction scheme. (Adopted).
- **A-OfP**: AoI-aware Offline Prediction scheme.
- **nA-OfP**: non-AoI-aware Offline Prediction scheme.

The above three optimization scheme yield different 1) radar TSC prediction value; 2) waveform power allocation optimization result; and 3) communication receiver threshold setting.

1) Online Prediction of Radar TSC: Fig. 8 shows the real value of TSC and the prediction value that is generated by different schemes in the last pulse, and Fig. 9 shows the mean square error of these three schemes over time. Note that the A-OfP and nA-OfP schemes both adopt the traditional MAP-based offline TSC estimation method, while the proposed A-OnP scheme adopts the online-based TSC estimation, as marked by the red line in Fig. 8. It is obvious in Fig. 8 that the online prediction method generates a more accurate value of TSC than the A-OfP-based method, which will contribute to radar performance compensation, that is because with the

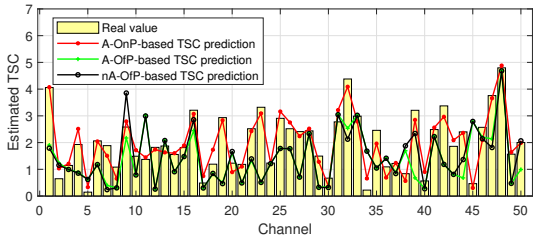

Fig. 8. TSC real value and estimated value under different schemes.

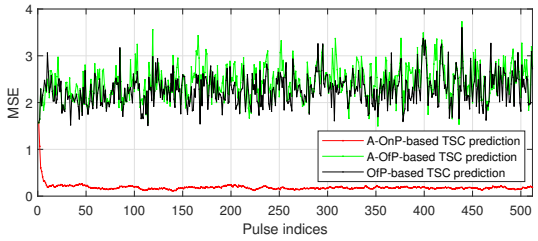

Fig. 9. Mean square error of TSC estimation under different schemes.

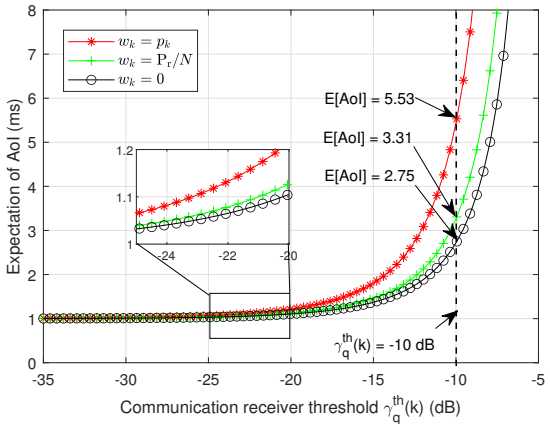

Fig. 10. Communication average AoI under radar interference.

closed-loop cognitive signal processing, the radar performance will be improved as the number of loops increases, as shown in Fig. 9, thus the estimated RMI will approach the true RMI when the TSC prediction accuracy increases, which would improve the reliability of decision.

2) AoI-aware Waveform Power Allocation: Firstly, we investigate the radar impact on the communication system. Fig. 10 shows the expectation of AoI under radar interference. To be specific, this figure shows the reachable AoI range of one channel versus communication receiver threshold. In order to rule out other possible causes of the outage difference, we conduct this experiment under fixed communication signal of $|s_{m,q}(k)|^2 = \frac{\mathrm{P_c}}{N_m}$ and assume a successful transmission of last pulse with $A_{q-1}(k) = T$, leaving the radar signal power of this chosen channel the only variable that differs. As shown in Fig. 10, the expectation of AoI can be raised up at any threshold setting, and this impact becomes more and more notable as γ_k increases. Take $\gamma_k = -10\mathrm{dB}$ as an example, where the expectation of AoI can be lifted into

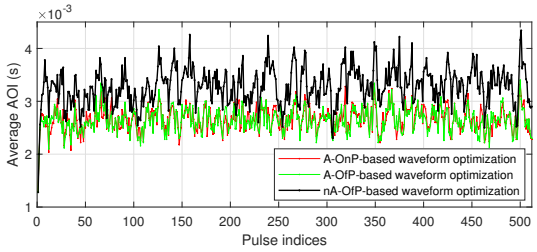

Fig. 11. Communication average AoI under different waveform power allocation schemes.

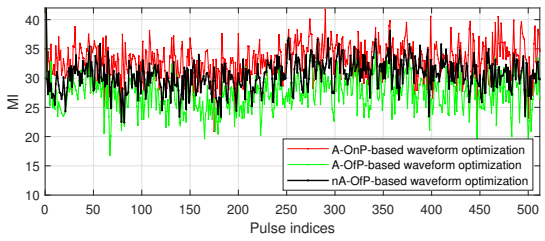

Fig. 12. Radar mutual information under different waveform power allocation schemes.

5.53 PRIs, in contrast to 2.75 PRIs under a radar-interference-free circumstance and 3.31 PRIs under the radar interference of evenly power distribution. In other words, the bigger the threshold value is, the greater impact radar shows on the AoI performance of communication channels. By analyzing (12) and Fig. 10, it is noticeable that radar power distribution has considerable influence on the communication sub-system, a small change in radar power allocation could cause a remarkable AoI fluctuation. Moreover, this influence will be more and more significant as the receiver threshold increases.

Fig. 11 and Fig. 12 show the average AoI of all communication users and the RMI of the radar system versus pulse indices, respectively. As shown in Fig. 11, the optimal waveform generated by the nA-OfP scheme has the worst AoI over the three schemes, because the impact of radar interference on the freshness of communication data has not been taken into consideration. In contrast, the optimal waveform generated by the A-OnP and A-OfP schemes manage to get an average AoI decrease by strengthening restrictions on radar waveform design process. Meanwhile, A-OfP scheme suffers a penalty in the RMI performance, as shown in Fig. 12, while A-OnP scheme can achieve higher RMI than the other two schemes with maintaining the AoI advantage, that is because the online TSC prediction provides additional benefits on the waveform optimization process by offering a more accurate TSC value for RMI calculation.

3) Adaptive Communication Receiver Threshold Adjustment: Fig. 13 and Fig. 14 show the average AoI of all communication users and the RMI of the radar system versus pulse indices under different communication threshold settings, respectively. As shown in Fig. 13, the threshold value set by the A-OnP scheme shows the best AoI performance, which has the lowest value and the smoothest curve, suggesting more fresh information and more stable data transmission. Besides, as shown in Fig. 14, the A-OnP scheme also indicates the

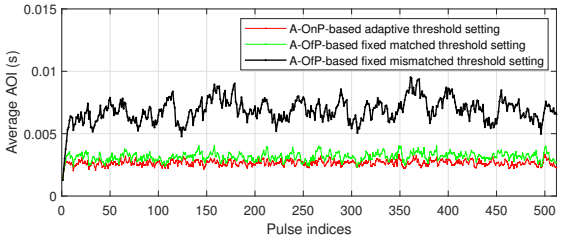

Fig. 13. Communication average AoI under different threshold setting schemes.

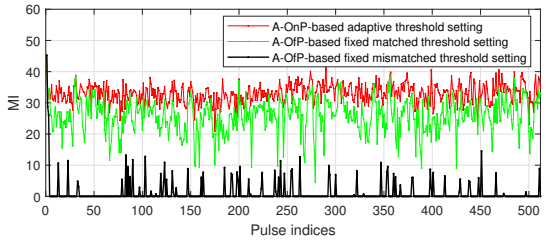

Fig. 14. Radar mutual information under different threshold setting schemes.

highest value of RMI, that is because under the premise of the cooperative JRC framework, the AoI of the last pulse will effect the waveform design process of the current pulse, a larger AoI indicates a stronger suppression against the radar waveform. Through the black line in Fig. 13-14, we can confirm our previous inference in Section III that if the settings of the communication threshold and relevant parameters can not keep (12b) hold, the waveform optimization solution will be setting the radar signal power completely to zero as AoI increases, which in turn causes a severe suppression on radar performance, as illustrated by the black line in Fig. 14.

In summery, the A-OnP scheme guarantees a small and stable value of AoI for each user, while the A-OfP scheme with a fixed matched threshold can guarantee the stability of the system but can not keep the AoI value at a small level. In other words, every communication user will eventually have a connection with the base station after some delay and re-transmission, so after all, the data exchange is ensured. But the A-OfP scheme with a fixed mismatched value would trigger a dire situation that the AoI of each user continues to rise and the radar signal gets suppressed over and over again.

VI. Conclusion

In this paper, we have investigated a JRC system with shared spectrum between radar and communication sub-systems for mitigating RF congestion in future related applications. We propose a fully-cooperative framework for the JRC system and consider a new network performance metric, AoI, to measure the freshness of data on communication terminals. Mathematical and simulation results show that the radar waveform can have a significant impact on the communication AoI performance, designing radar waveform accordingly can reduce the interference, but it comes at the cost of radar performance loss. Effective performance compensation can be achieved through cognitive signal processing on radar side.

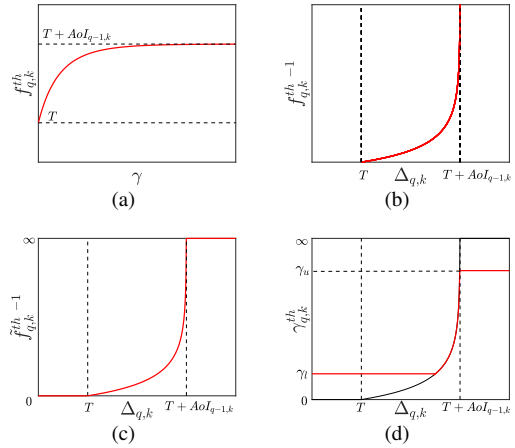

Fig. 15. Transformation from fuction (24) to equation (25)

Besides, adjusting communication threshold adaptively with respect to radar waveform can avoid performance suppression on both communication and radar sides. The proposed CS-CD method resolves the multi-variable non-convex problem effectively, with simulation results showing a decrease in AoI and an increase in RMI at the same time, which verifies the advantage of our proposed cooperative JRC framework and the effectiveness of the proposed CS-CD method.

Appendix

Proof of Lemma 2

The derivative of function (24) can be written as:

$$\begin{aligned}\frac{\mathrm{d}f_{q,k}^{th}(\gamma)}{\mathrm{d}\gamma} &= \frac{\mathrm{d}\left[\mathrm{T}+\left(1-\frac{\mathrm{e}^{-\rho_1\gamma}}{1+\rho_2\gamma}\right)\mathrm{A_{q-1}(k)}\right]}{\mathrm{d}\gamma} \\ &= A_{q-1}(k)\mathrm{e}^{-\rho_1\gamma}\left[\frac{\rho_1}{1+\rho_2\gamma}+\frac{\rho_2}{(1+\rho_2\gamma)^2}\right].\end{aligned} \tag{37}$$

(37) is always larger than zero because it has always been hold that $A_{q-1}(k) \geq T$, $\mathrm{e}^{-\rho_1\gamma} > 0$, $1+\rho_2\gamma \geq 1$, $\rho_1 > 0$ and $\rho_2 \geq 0$ that means $f_{q,k}^{th}(\gamma)$ is a positive monotonically increasing function, as illustrated by Fig. 15 (a), which is consistent with the fact that the outage probability will continue to grow as the receiver thrershold increses. Thus the infimum of $f_{q,k}^{th}(\gamma)$ can be obtained by (38), and the upper bound of $f_{q,k}^{th}(\gamma)$ can be obtained by (39). It is noticeable that its inverse function ${f_{q,k}^{th}}^{-1}$ is also a positive monotonically increasing function, as illustrated by Fig. 15 (b).

$$\inf\left[f_{q,k}^{th}(\gamma)\right] = f_{q,k}^{th}(0) = T, \tag{38}$$

$$\max\left[f_{q,k}^{th}(\gamma)\right] = \lim_{\gamma\to\infty} f_{q,k}^{th}(\gamma) = T + AoI_{q-1}(k). \tag{39}$$

We define the extended-value extension of the inverse function of $f_{q,k}^{th}(\gamma)$ as:

$$\tilde{f}_{q,k}^{th\,-1}(\Delta_{q,k}) \triangleq \begin{cases} 0, & \Delta_{q,k} < \inf\left[f_{q,k}^{th}(\gamma)\right], \\ {f_{q,k}^{th}}^{-1}(\Delta_{q,k}), & \Delta_{q,k} \in \mathbf{dom}\ {f_{q,k}^{th}}^{-1}, \\ \infty, & \Delta_{q,k} \geq \max\left[f_{q,k}^{th}(\gamma)\right], \end{cases} \tag{40}$$

where $\mathbf{dom}\ {f_{q,k}^{th}}^{-1} = [T, T + AoI_{q-1}(k))$ denotes the domain of ${f_{q,k}^{th}}^{-1}(\Delta_{q,k})$, or the range of $f_{q,k}^{th}(\gamma)$. The extended-value extension does not break the monotonicity of the original function, thus ${\tilde{f}_{q,k}^{th}}^{-1}$ is still a monotone non-decreasing function, as illustrated by Fig. 15 (c).

Thus (25) is a fragment of ${f_{q,k}^{th}}^{-1}$, truncated by the lower and upper numerical bounds, and can be illustrated by Fig. 15 (d), which apparently is a monotone non-decreasing function.

REFERENCES

[1] Y. Cui, F. Liu, X. Ling, and J. Mu, "Integrating sensing and communications for ubiquitous IoT: Applications, trends, and challenges," *IEEE Network*, vol. 35, no. 5, pp. 158–167, Sep. 2021.

[2] J. A. Zhang, M. L. Rahman, K. Wu, X. Huang, Y. J. Guo, S. Chen, and J. Yuan, "Enabling joint communication and radar sensing in mobile networks—A survey," *IEEE Commun. Surveys Tuts.*, vol. 24, no. 1, pp. 306–345, Oct. 2021.

[3] F. Liu, Y. Cui, C. Masouros, J. Xu, T. X. Han, Y. C. Eldar, and S. Buzzi, "Integrated sensing and communications: Toward dual-functional wireless networks for 6G and beyond," *IEEE J. Sel. Areas in Commun.*, vol. 40, no. 6, pp. 1728–1767, Jun. 2022.

[4] F. Liu, C. Masouros, A. P. Petropulu, H. Griffiths, and L. Hanzo, "Joint radar and communication design: Applications, state-of-the-art, and the road ahead," *IEEE Trans. Commun.*, vol. 68, no. 6, pp. 3834–3862, Jun. 2020.

[5] C. Sturm and W. Wiesbeck, "Waveform design and signal processing aspects for fusion of wireless communications and radar sensing," *Proc. IEEE*, vol. 99, no. 7, pp. 1236–1259, Jul. 2011.

[6] R. F. Tigrek, W. J. A. De Heij, and P. Van Genderen, "OFDM signals as the radar waveform to solve Doppler ambiguity," *IEEE Trans. Aerosp. Electron. Syst.*, vol. 48, no. 1, pp. 130–143, Jan. 2012.

[7] T. Xu, F. Liu, C. Masouros, and I. Darwazeh, "An experimental proof of concept for integrated sensing and communications waveform design," *IEEE Open J. Commun. Soc.*, vol. 3, pp. 1643–1655, Sep. 2022.

[8] M. Temiz, E. Alsusa, and M. W. Baidas, "A dual-functional massive MIMO OFDM communication and radar transmitter architecture," *IEEE Trans. Veh. Technol.*, vol. 69, no. 12, pp. 14 974–14 988, Dec. 2020.

[9] J. Chapin, "Shared spectrum access for radar and communications (SSPARC)," *DARPA BBA-13-24 www.darpa.mil*, 2012.

[10] Y. He, Y. Cai, G. Yu, and K.-K. Wong, "Joint transceiver design for dual-functional full-duplex relay aided radar-communication systems," *IEEE Trans. Commun.*, vol. 70, no. 12, pp. 8355–8369, Dec. 2022.

[11] F. Gao, L. Xu, and S. Ma, "Integrated sensing and communications with joint beam-squint and beam-split for mmWave/THz massive MIMO," *IEEE Trans. Commun.*, vol. 71, no. 5, pp. 2963–2976, May 2023.

[12] Y. Xiong, F. Liu, Y. Cui, W. Yuan, T. X. Han, and G. Caire, "On the fundamental tradeoff of integrated sensing and communications under gaussian channels," *IEEE Trans. Inf. Theory*, vol. 69, no. 9, pp. 5723–5751, Sep. 2023.

[13] Q. Zhang, H. Sun, X. Gao, X. Wang, and Z. Feng, "Time-division ISAC enabled connected automated vehicles cooperation algorithm design and performance evaluation," *IEEE J. Sel. Areas in Commun.*, vol. 40, no. 7, pp. 2206–2218, Jul. 2022.

[14] C. Shi, Y. Wang, F. Wang, S. Salous, and J. Zhou, "Joint optimization scheme for subcarrier selection and power allocation in multicarrier dual-function radar-communication system," *IEEE Syst. J.*, vol. 15, no. 1, pp. 947–958, Mar. 2021.

[15] X. Chen, Z. Feng, Z. Wei, P. Zhang, and X. Yuan, "Code-division OFDM joint communication and sensing system for 6G machine-type communication," *IEEE Internet of Things J.*, vol. 8, no. 15, pp. 12 093–12 105, Aug. 2021.

[16] T. Tian, T. Zhang, L. Kong, and Y. Deng, "Transmit/receive beamforming for MIMO-OFDM based dual-function radar and communication," *IEEE Trans. Veh. Technol.*, vol. 70, no. 5, pp. 4693–4708, May 2021.

[17] W. Zhou, R. Zhang, G. Chen, and W. Wu, "Integrated sensing and communication waveform design: A survey," *IEEE Open J. Commun. Soc.*, vol. 3, pp. 1930–1949, Oct. 2022.

[18] M. Bell, "Information theory and radar waveform design," *IEEE Trans. Inf. Theory*, vol. 39, no. 5, pp. 1578–1597, Sep. 1993.

[19] Y. Yang and R. S. Blum, "MIMO radar waveform design based on mutual information and minimum mean-square error estimation," *IEEE Trans. Aerosp. Electron. Syst.*, vol. 43, no. 1, pp. 330–343, Jan. 2007.

[20] F. Wang, H. Li, and M. A. Govoni, "Power allocation and co-design of multicarrier communication and radar systems for spectral coexistence," *IEEE Trans. Signal Process.*, vol. 67, no. 14, pp. 3818–3831, Jul. 2019.

[21] K.-W. Huang, M. Bică, U. Mitra, and V. Koivunen, "Radar waveform design in spectrum sharing environment: Coexistence and cognition," in *Proc. IEEE Radar Conf. (RadarCon)*, May 2015, pp. 1698–1703.

[22] Bosung Kang and M. Rangaswamy, "Radar waveform design under communication sum capacity constraint," *IEEE Trans. Signal Process.*, vol. 69, pp. 2795–2806, May 2021.

[23] T. Tian, G. Li, and T. Zhou, "Power distribution for an OFDM-based dual-function radar-communication sensor," *IEEE Sens. Lett.*, vol. 4, no. 11, pp. 1–4, Nov. 2020.

[24] Y. Sun, E. Uysal-Biyikoglu, R. D. Yates, C. E. Koksal, and N. B. Shroff, "Update or wait: How to keep your data fresh," *IEEE Trans. on Inf. Theory*, vol. 63, no. 11, pp. 7492–7508, Nov. 2017.

[25] C. Kam, S. Kompella, and A. Ephremides, "Experimental evaluation of the age of information via emulation," in *Proc. IEEE MILCOM, Tampa, FL, USA*, Oct. 2015, pp. 1070–1075.

[26] J. Lee, D. Niyato, Y. L. Guan, and D. I. Kim, "Learning to schedule joint radar-communication requests for optimal information freshness," in *Proc. IEEE Intell. Vehicles Symp. (IV)*, Jul. 2021, pp. 8–15.

[27] J. Liu, S. He, L. Zhang, Y. Zhang, G. Zhu, H. Yin, and H. Yan, "An automatic and forward method to establish 3-D parametric scattering center models of complex targets for target recognition," *IEEE Trans. Geosci. Remote Sens.*, vol. 58, no. 12, pp. 8701–8716, Dec. 2020.

[28] Z. Zhao, X. Tang, and Y. Dong, "Cognitive waveform design for dual-functional MIMO radar-communication systems," in *Proc. IEEE Glob. Commun. Conf. (GLOBECOM)*, Dec. 2022, pp. 5607–5612.

[29] J. Chen, X. Wang, and Y.-C. Liang, "Impact of channel aging on dual-function radar-communication systems: Performance analysis and resource allocation," *IEEE Trans. Commun.*, vol. 71, no. 8, pp. 4972–4987, Aug. 2023.

[30] Y. Yao and L. Wu, "Cognitive waveform design for radar-communication transceiver networks," *J. Adv. Transp.*, vol. 2018, Apr. 2018.

[31] R. A. Romero and N. A. Goodman, "Waveform design in signal-dependent interference and application to target recognition with multiple transmissions," *IET Radar, Sonar Navig.*, vol. 3, no. 4, pp. 328–340, Aug. 2009.

[32] F. Liu, C. Masouros, and Y. C. Eldar, Eds., *Integrated Sensing and Communications*. Singapore: Springer Nature Singapore, 2023.

[33] "Summary of Rel-15 Work Items," 3rd Generation Partnership Project, 2018.

[34] P. Chen, C. Qi, L. Wu, and X. Wang, "Waveform design for Kalman filter-based target scattering coefficient estimation in adaptive radar system," *IEEE Trans. on Veh. Technol.*, vol. 67, no. 12, pp. 11 805–11 817, Dec. 2018.

[35] X. Zhang and C. Cui, "Range-spread target detecting for cognitive radar based on track-before-detect," *Int. J. Electron.*, vol. 101, no. 1, pp. 74–87, Jan. 2014.

[36] F. Z. Dai, H. W. Liu, P. H. Wang, and S. Z. Xia, "Adaptive waveform design for range-spread target tracking," *Electron. Lett.*, vol. 46, no. 11, pp. 1–2, May 2010.

[37] X. Fengming, W. Jinkuan, W. Bin, and S. Xin, "Waveform design for cognitive radar based on information theory," in *Proc. 2022 IEEE International Conf. on Multisensor Fusion and Integration for Intelligent Systems (MFI)*, Sep. 2014, pp. 1–8.

[38] Z. Zhang, Z. Du, and W. Yu, "Mutual-information-based OFDM waveform design for integrated radar-communication system in Gaussian mixture clutter," *IEEE Sens. Lett.*, vol. 4, no. 1, Jan. 2020.

[39] M. Bică and V. Koivunen, "Radar waveform optimization for target parameter estimation in cooperative radar-communications systems," *IEEE Trans. Aerosp. Electron. Syst.*, vol. 55, no. 5, pp. 2314–2326, Oct. 2019.

[40] S. P. Boyd and L. Vandenberghe, *Convex Optimization*. Cambridge University Press, Mar. 2004.

Zhuofei Li (Graduate Student Member, IEEE) received the B.S. degree in the College of Communication Engineering, Jilin University, Jilin, China, in 2019. She is currently pursuing the Ph.D degree in Jilin University, Jilin, China. She was a visiting Ph.D. student in the Faculty of Information Technology, University of Jyväskylä, Jyväskylä, Finland, in 2022. Her research interests include integrated sensing and communication, resource allocation, convex optimization, and vehicular networks.

Fengye Hu (M'12-SM'21) received the B.S. degree from the Department of Precision Instrument, Xian University of Technology (China) in 1996, and the M.S. and Ph.D. degrees in communication and information systems from Jilin University, China, in 2000 and 2007, respectively. He served as a visiting scholar in electrical and electronic engineering from Nanyang Technological University (NTU), Singapore, in 2011. He is currently a full professor in the College of Communication Engineering, Jilin University. His current research interests include wireless body area networks, wireless energy and information transfer, energy harvesting, cognitive radio, and space–time communication. He is an Editor of IEEE TVT, IEEE IOTJ and China Communications, and served as an Editor of IET Communications. He has published 80+ publications in IEEE journals and conferences. He organized the first and second Asia-Pacific Workshop on Wireless Networking and Communications (APWNC 2013 and APWNC 2015). He also organized the Future 5G Forum on Wireless Communications and Networking Big Data (FWCN 2016), Workshop on Integration of Communication, Sensing and Computing in Next Generation Mobile Communications Network (CSCN 2022), and Workshop on Frontier Technologies of Detection, Communication and Computing in Next Generation Network (DCCN 2023). He served as an Executive Co-Chairs of IEEE/CIC International Conference on Communications in China (ICCC), China, in 2019.

Qihao Li (M'16) received the M.Sc. degree in Information and Communication Technology from University of Agder, Norway, in 2014 and received his Ph.D. degree in University of Oslo, Norway, in 2019. After that, he was a postdoctoral fellow with the Department of Electrical and Computer Engineering, University of Waterloo, from 2019 to 2021, and a lecturer with the School of Electrical Engineering and Intelligentization, Dongguan University of Technology, from 2022 to 2023. Since 2023, he has been an assoicate professor at Jilin University, China. His current research focuses on industrial Internet, digital twin, optimal control and optimization, wireless network security and localization. He served as an Associate Editor for the IEEE INTERNET OF THIGNS JOURNAL. He also servers/served as the TPC Chair for IEEE CIC/ICCC' 23-24, and members of TPC for IEEE Globecom'19-24, IEEE ICC'19-24, IEEE CIC ICCC'17-24, EuCAP'2019, BDEC-SmartCity'18

Zhuang Ling (Member, IEEE) received the B.S. and Ph.D. degrees in the College of Communication Engineering, Jilin University, Jilin, China, in 2016 and 2021, respectively. He is a Postdoctoral Fellow in the College of Communication Engineering, Jilin University, Changchun, Jilin, China. He was a visiting Ph.D. student with the Department of Electrical and Computer Engineering at the University of Houston in 2019. His research interests include Wireless Body Area Network, High Speed Railway, Backscatter Communications, Energy Harvesting, Age of Information, and Distributionally Robust Optimization.

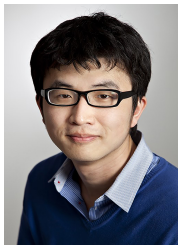

Zheng Chang (S'10-M'13-SM'17) received the B.Eng. degree from Jilin University, Changchun, China in 2007, M.Sc. (Tech.) degree from Helsinki University of Technology (Now Aalto University), Espoo, Finland in 2009 and Ph.D degree from the University of Jyväskylä, Jyväskylä, Finland in 2013. From 2008-2021, he has held various research positions at Aalto University, University of Jyvaskyla and Magister Solutions Ltd in Finland. He serves as an editor of IEEE Wireless Communications Letters, Springer Wireless Networks and China Communications, and a guest editor for IEEE Network, IEEE Wireless Communications, IEEE Communications Magazine, IEEE Internet of Things Journal, etc. He has been awarded as 2018 IEEE Communications Society best young researcher for Europe, Middle East and Africa Region and 2021 IEEE Communications Society MMTC Outstanding Young Researcher. He has published over 160 papers in journals and conferences, and received best paper awards from IEEE ICC in 2023, TCGCC and APCC in 2017. His research interests include IoT, cloud/edge computing, security and privacy, vehicular networks, and green communications.

Timo Hämäläinen (Senior Member, IEEE) has over 25 year's experience of the computer networks. He has more than 250 internationally peer reviewed publications and he has supervised more than 40 Ph.D. theses. His research interests include performance evaluation and management of telecommunication networks, and in particular resource allocation, quality of service, anomaly detection, and network security. He is currently leading a research group in the area of network resource management and anomaly detection with the IT Faculty, University of Jyväskylä. He is a board member of this area's journals and IEEE conferences.